P H Y S I C A L   R E V I E W   L E T T E R S

How to Capture Active Particles

A. Kaiser,[1] H. H. Wensink,[1,2,*] and H. Löwen[1]

[1]*Institut für Theoretische Physik II: Weiche Materie, Heinrich-Heine-Universität Düsseldorf,
Universitätsstrasse 1, D-40225 Düsseldorf, Germany*
[2]*Laboratoire de Physique des Solides, Université Paris-Sud and CNRS, 91405 Orsay, France*
(Received 20 January 2012; published 29 June 2012)

In many applications, it is important to catch collections of autonomously navigating microbes and man-made microswimmers in a controlled way. Using computer simulation of a two-dimensional system of self-propelled rods we show that a static chevron-shaped wall represents an excellent trapping device for self-motile particles. Its catching efficiency can be controlled by varying the apex angle of the trap which defines the sharpness of the cusp. Upon decreasing the angle we find a sequence of three emergent states: no trapping at wide angles followed by a sharp transition towards complete trapping at medium angles and a crossover to partial trapping at small cusp angles. A generic trapping "phase diagram" maps out the conditions at which the capture of active particles at a given density is rendered optimal.

One of the key survival strategies of human beings over the ages is their ability to catch animals. An efficient way to capture mammals, fish and birds is "trapping," i.e., releasing a device in a populated zone which irreversibly attracts and stores the prey. While the methods for capturing (macroscopic) animals have been well optimized by now, the corresponding problem in the microworld, namely catching microbes, is much more challenging due to the strongly reduced nanometric size of the trap. The possibility to trap autonomously navigating microorganisms in a controlled way provides fascinating options to prevent or cure microbial contamination [1,2] and to concentrate microbes near externally imposed patterned surfaces [3]. Similar applications can be envisaged for man-made microswimmers, i.e., artificial particles which are actively propagating due to an internal "motor". Examples include catalytically driven Janus particles [4–6], colloids with artificial flagella [7,8] and vibrated granulates [9,10]. Lithographic techniques have been employed to confine, control and steer the motion of microbes and artificial microswimmers [11,12]. The use of lithographic nanopatterns has advanced significantly in recent years [13,14] and has opened up numerous possibilities to sort particles [15,16], to rectify their motion [3,17], and to design building blocks of micromachines [18–20]. These experimental observations provide impetus for devising models which can explain collective self-trapping of active particles. These models may subsequently serve as benchmarks for the design of efficient microbial traps.

It is well known that (passive) fluids in strong confinement behave quite differently from the bulk. In this Letter we explore the dramatic effect of system boundaries for active fluids. In particular, we utilize geometric confinement to propose an efficient strategy for capturing rigid self-propelled rods (SPR) in which particles are exposed to a simple static boundary of variable shape. The collective behavior of SPRs is simulated using a two-dimensional, particle-resolved model which predicts the formation of swarms in bulk. The presence of a static chevron-type boundary with variable apex angle leads to collective rectification of particle motion and eventually to a pronounced self-trapping at the trap boundary. The apex angle α of the chevron plays a key role in determining the self-trapping efficiency of the setup and unveils three distinct nonequilibrium stationary states: no trapping, partial trapping, and complete trapping. The transition from partial to complete trapping occurs smoothly at a lower critical angle while the complete trapping state abruptly terminates at an upper critical apex angle. We show that the sharp transition from complete to no trapping at large apex angles has an appropriate system-size scaling which allows a classification similar to a true thermodynamic phase transition. Collective self-trapping emerges as a generic many-body effect which is found to be robust against intrinsic rotational fluctuations of the microswimmers. The phenomenon is therefore expected to be relevant to a large range of self-motile microparticles in planar confinement as well as 3D bulk situations.

Our model consists of N rigid rods of length ℓ, each with a constant self-motility force F_a directed along the main axis. Due to solvent friction the particles move in the overdamped low Reynolds number regime, while interacting with the other particles and the boundary by steric forces only [21]. The latter are implemented by discretizing each rod into a linear array of n equidistant spherical segments and imposing a repulsive Yukawa potential between the segments of each pair. The total pair potential between rods $\{\alpha, \beta\}$ with orientational unit vectors $\{\hat{\mathbf{u}}_\alpha, \hat{\mathbf{u}}_\beta\}$ and centre of mass distance $\Delta\mathbf{r}_{\alpha\beta}$ is then given by $U_{\alpha\beta} = (U_0/n^2)\sum_{i=1}^{n}\sum_{j=1}^{n}\exp[-r_{ij}^{\alpha\beta}/\lambda]/r_{ij}^{\alpha\beta}$, where $U_0 > 0$ defines the amplitude, λ the screening length and $r_{ij}^{\alpha\beta} = |\Delta\mathbf{r}_{\alpha\beta} + (l_i\hat{\mathbf{u}}_\alpha - l_j\hat{\mathbf{u}}_\beta)|$ the distance between

segment i of rod α and j of rod β ($\alpha \neq \beta$) with $l_i = d(i-1)$, $i \in [1, n]$ denoting the segment position along the main rod axis. The number of rod segments n is chosen such that the intrarod segment distance $d = \ell/(n-1) \leq \lambda$ and rod overlaps are prevented. A trap is introduced as a static boundary with a prescribed shape and contour length ℓ_T. Particle-trap interactions are implemented by discretizing the trap boundary into $n_T = \lfloor \ell_T/d \rfloor$ equidistant segments each interacting with the rod segments via the same Yukawa potential. Mutual SPR collisions generate apolar nematic alignment which stimulates swarm formation at finite concentrations [10]. The boundary potential mimics a hard wall and imparts 2D planar order with rods pointing favorably perpendicular to the local wall normal.

The microscopic equations of motion for the positions and orientations of the SPRs emerge from a balance of the forces and torques acting on each rod α,

$$\mathbf{f}_{\mathcal{T}} \cdot \partial_t \mathbf{r}_\alpha(t) = -\nabla_{\mathbf{r}_\alpha} U(t) + F_a \hat{\mathbf{u}}_\alpha(t),$$
$$\mathbf{f}_{\mathcal{R}} \cdot \partial_t \hat{\mathbf{u}}_\alpha(t) = -\nabla_{\hat{\mathbf{u}}_\alpha} U(t) + \mathbf{M}_\alpha(t),$$
(1)

in terms of the total potential energy $U = (1/2)\sum_{\alpha,\beta(\alpha \neq \beta)} U_{\alpha\beta} + \sum_{\alpha,T} U_{\alpha T}$ with $U_{\alpha T}$ the potential energy of rod α with the trap. The one-body translational and rotational friction tensors $\mathbf{f}_{\mathcal{T}}$ and $\mathbf{f}_{\mathcal{R}}$ can be decomposed into parallel, perpendicular and rotational contributions which depend solely on the aspect ratio $a = \ell/\lambda$ [22]. The typical self-propulsion speed of a single rod $v_0 = F_a/\|\mathbf{f}_{\mathcal{T}}\|$ defines the time interval $\tau = \ell/v_0$ a SPR needs to swim a distance comparable to its size. Orientational fluctuations induced by, e.g., bacterial tumbling are represented by a stochastic torque $\mathbf{M}_\alpha$ with zero mean $\langle M_{i\alpha}(t) \rangle = 0$ and correlations $\langle M_{i\alpha}(t)M_{j\beta}(t') \rangle = 2D_{\mathcal{R}}\|\mathbf{f}_{\mathcal{R}}\|^2 \delta_{ij}\delta_{\alpha\beta}\delta(t - t')$ ($i = x, y$) with $D_{\mathcal{R}}$ an effective rotational diffusion rate. The strength of the rotational fluctuations is given by the parameter $\gamma = \ell D_{\mathcal{R}}/v_0$ which allows interpolation between noiseless, directed SPR motion ($\gamma = 0$) and "run and tumble" motion ($\gamma > 0$) as observed for *E. coli* and other bacterial species [23,24].

We simulate SPRs with aspect ratio $a = 10$ in a rectangular simulation box with area A and periodic boundary conditions in both Cartesian directions. A particle packing fraction is defined as $\phi = N\sigma/A$ with $\sigma = \ell\lambda + \lambda^2\pi/4$ the effective area of a single rod. In the bulk density range $\phi < 0.2$ the SPRs spontaneously form flocks with strong spatial density fluctuations [25]. Let us now subject the SPRs to a chevron boundary with contour length $\ell_T = 20\ell$ and variable apex angle $0° < \alpha < 180°$ (see Fig. 1). In the macroscopic limit, the system can be interpreted as a reservoir of microswimmers exposed to an equidistant array of mutually independent static traps. The area fraction occupied by the traps is angle dependent with a maximum value given by $\phi_T = (\ell_T^2/8A)$ which fixes the number of rods via $N = (\ell_T^2/8\sigma)(\phi/\phi_T)$. We constrain $\phi_T < 0.1$ in order to guarantee the traps to be completely
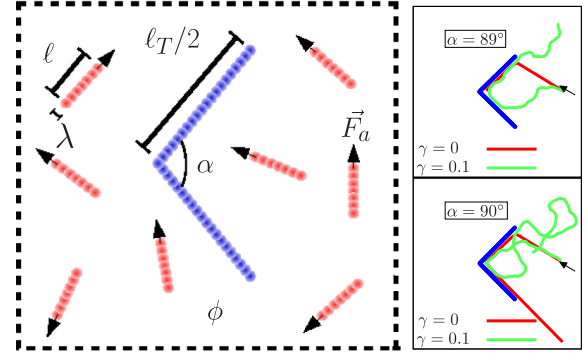

FIG. 1 (color online). Sketch of a system of SPRs with aspect ratio $a = \ell/\lambda$ and axial active force F_a at bulk density ϕ subjected to a static chevron-type trap with contour length ℓ_T and apex angle α. The macroscopic system consists of periodic replicas with boundaries indicated by the dotted lines. Real-space trajectories of a single SPR with(out) rotational noise are shown on the right. Arrows mark the initial SPR configuration. A noiseless SPR ($\gamma = 0$) gets trapped if $\alpha < 90$.

independent of each other within the typical range of bulk rod packing fractions $0 < \phi < 0.1$ considered here. A SPR is considered trapped if its velocity $v = |\mathbf{v}|$ remains below a threshold value v^* during a time interval of at least $t^* = 25\tau$. The number fraction of trapped rods defines the trapping efficiency $x_T(t) = N_T(t)/N$ and its long-time limit $x_T^{(0)} = \lim_{t\to\infty} x_T(t)$ ($0 \leq x_T^{(0)} \leq 1$) can be used to discern various stationary states.

Figure 2(a) represents an overview of the collective trapping states for noiseless SPRs ($\gamma = 0$) that emerge upon varying the two main system variables, the rod packing fraction ϕ, and trap angle α. The trapping "phase diagram" exhibits three distinct stationary regimes. First, for large α no trapping occurs as the cusp is too wide to efficiently capture a significant fraction of particles in the system. Second, below a certain critical angle a sharp transition towards complete trapping occurs. This state is characterized by the formation of a large monocluster comprising all particles in the system. Upon further decreasing α a third region is entered corresponding to partial trapping. In this regime, the effective rod-trap collision cross section is insufficient to trap all the particles present in the system, and a substantial portion of rods remains mobile even at large t. The transitions demarcating the various states in the diagram can be inferred from the evolution of the trapping "order parameter" $x_T^{(0)}$ as a function of α, as shown in Fig. 3(a). Upon departing from the flat-wall limit a sharp discontinuity occurs around $\alpha \sim 120°$ where the jump in $x_T^{(0)}$ from zero to unity signals a transition from no trapping to complete trapping. For sharper cusps a second, continuous transition from complete to partial trapping can be located at the point where $x_T^{(0)}$ starts dropping smoothly below unity. The sharp transition toward complete trapping is only marginally affected by the rotational fluctuations [Fig. 3(b)], although
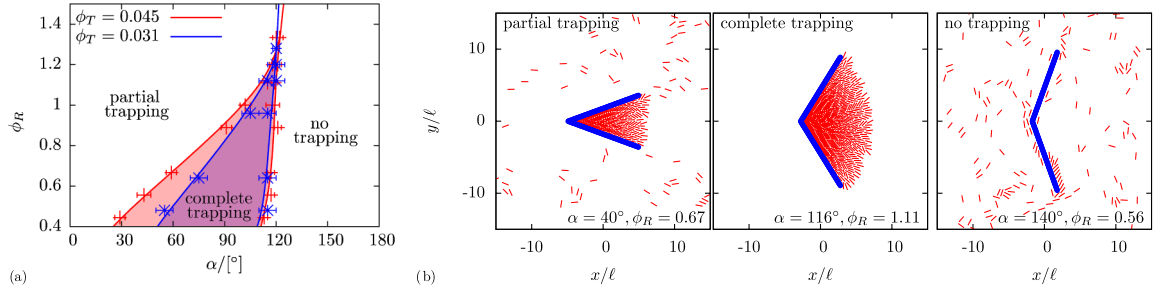
FIG. 2 (color online).   (a) Phase diagram marking three different collective trapping states of SPRs ($\gamma = 0$) at a chevron boundary with length $\ell_T = 20\ell$; no trapping at large apex angle α, complete trapping at medium α and partial trapping at small α upon variation of the reduced rod packing fraction $\phi_R = \phi/\phi_T$. Phase boundaries are shown for two different values of ϕ_T; the area fraction occupied by the trap. The region of complete trapping is bounded by a triple point at larger rod concentration beyond which a smooth transition from no trapping to partial trapping occurs. (b) Snapshots depicting the three stationary states for the case $\phi_T = 0.045$.

the individual particle trajectories are quite different (Fig. 1). The robustness of $x_T^{(0)}$ with respect to the choice of v^* can be established from the velocity histograms $P(v)$ in Fig. 3(c) whose strongly bimodal character provides an unambiguous distinction between trapped and mobile SPRs. Also here, the collective properties appear rather insensitive to γ for typical bacterial values $\gamma \simeq 0.01$ [24].

It is worth noting from Fig. 2(a) that the transition from no trapping to complete trapping is fairly insensitive to the rod concentration as well the area fraction occupied by
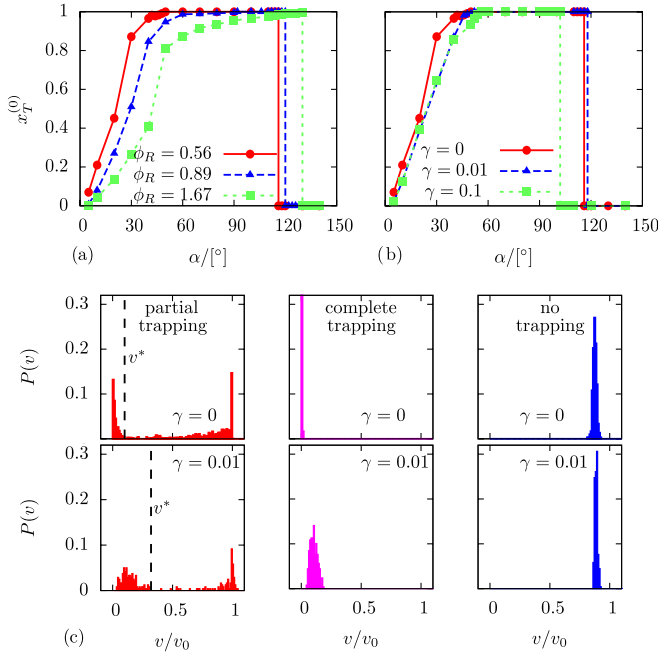

FIG. 3 (color online).   (a) Long-time trapping efficiency $x_T^{(0)}$ of noiseless ($\gamma = 0$) SPRs as a function of the trap angle α for three reduced rod packing fractions ϕ_R. The jumps around $\alpha = 120°$ signal "first-order" phase transitions from no trapping to complete trapping. (b) Same results for three different strengths of the rotational noise γ at $\phi_R = 0.56$. (c) Histograms of the normalized distribution $P(v)$ of SPR velocities v corresponding to the three trapping states for both deterministic and diffusive SPR motion.

trap. Generically, complete trapping is possible only if the apex angle does not exceed a typical threshold value $\alpha \approx 120°$. By defining a reduced rod density $\phi_R = \phi/\phi_T$ the triple point is rendered virtually independent of the trap area fraction and attains a universal value $\phi_R^* \approx 1.3$. This suggests that the window of stability for complete trapping, as marked by the rod density ϕ^* at the triple point, can be systematically tuned by changing the number of traps per area and/or the contour length ℓ_T of the boundary. Although complete trapping is strictly suppressed at $\phi > \phi^*$, the trapping efficiency x_T still shows a marked jump from zero to nearly 100% if the angle drops below about 120°. This indicates that the chevron wall continues to be a powerful trapping device at larger bulk concentrations.

To ascertain whether the chevron is indeed the optimal shape we compare its trapping efficiency with that of a circular trap with identical trap area $A_T = 52\ell^2$ and trap angle $\alpha = 110°$. A time series of the fraction of trapped particles reveals a distinct difference between the two trap shapes (Fig. 4). While the chevron induces a fast intake of particles into the trap surface leading up to a trapping efficiency of almost 100% (complete trapping) at large times, the circular one fails to capture a significant fraction of particles over time. The rounded shape of the circular trap does not facilitate particle-wall anchoring but instead forces clusters of particles to slide collectively along the trap interior. This leads to a process whereby the rods collectively enter and leave the interior of the trap, as indicated by the "bursts" in the number fraction of particles x_I inside the trap in Fig. 4. Its rhythmic nature is reflected by a peak in the power spectrum at a characteristic frequency which translates into a typical life time 212τ of a rod cluster inside the circle trap. The number fraction of immobile rods $x_T(t)$, however, remains practically zero throughout the sampled time interval in stark contrast to the chevron trap.

In conclusion, while there is a wealth of knowledge about trapping passive particles, such as colloids in optical tweezers or atoms in a Paul trap, it less obvious how active particles can be captured collectively. We have shown that
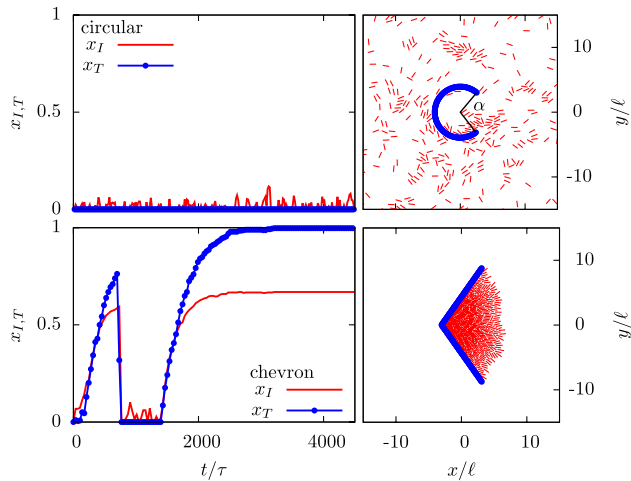
FIG. 4 (color online).   Comparison of the number fraction x_I of SPRs ($\gamma = 0$) located within the trap area and the fraction of trapped particles x_T as a function of time t for both chevron and circular traps with equal trap area $A_T = 52\ell^2$, angle $\alpha = 110°$ and reduced packing fraction $\phi_R = 0.89$.

active rods coherently self-trap at a static chevron-shaped boundary which enforces SPRs to rectify their swimming direction, jam at the cusp and form a small immobile cluster which subsequently acts as an efficient nucleus for growing a mesoscopic aggregate of trapped rods. The apex angle of the trap plays a crucial role in determining the stationary trapping state of the SPRs and reveals three emergent states: no trapping, partial trapping and complete trapping. A trap boundary which is rounded on the length scale of the particle extension is incapable of capturing particles over time. It is therefore essential for the trap boundary to possess sites with strong local curvature $\kappa \gg \ell^{-1}$ which serve as "nucleation" seeds for collective self-trapping. We remark that the trapping phenomenon can easily be envisaged in 3D situations where the trapping boundary is represented by a conical object. We further emphasize that the sharp transition from no trapping to complete trapping is a collective, nonequilibrium effect and is uncorrelated to self-trapping of a single SPR which depends sensitively on the level of noise (cf. the trajectories in Fig. 1). The dramatic collective response of SPRs to small changes in the boundary shape is remarkable and remains unseen for passive systems exposed to external boundaries or electromagnetic traps.

Collective trapping can be verified in experiments on rod-shaped bacteria [26] or driven polar granular rods [27] exposed to geometrically structured boundaries [12–14]. This setup could, for instance, be exploited as an efficient purification device to manipulate and remove contaminating microbes. Future challenges could focus on incorporating the effect of different propulsion mechanisms [28,29] and their associated hydrodynamic flow fields [30], as well as chemotactic forces mediated by local concentration variations of chemical substances. We believe, however,

that the long-ranged nature of these interactions will neither affect the microscopic mechanism underpinning collective trapping nor the global topology of the trapping phase diagram presented here.

*wensink@lps.u-psud.fr

 [1] E. C. Redmond and C. J. Griffith, J. Food Prot. **66**, 130 (2003).
 [2] J. Taylor, K. Lai, M. Davies, D. Clifton, I. Ridley, and P. Biddulph, Environ. Int. **37**, 1019 (2011).
 [3] P. Galajda, J. Keymer, P. Chaikin, and R. Austin, J. Bacteriol. **189**, 8704 (2007).
 [4] R. Golestanian, T. B. Liverpool, and A. Ajdari, Phys. Rev. Lett. **94**, 220801 (2005).
 [5] A. Erbe, M. Zientara, L. Baraban, C. Kreidler, and P. Leiderer, J. Phys. Condens. Matter **20**, 404215 (2008).
 [6] J. Palacci, C. Cottin-Bizonne, C. Ybert, and L. Bocquet, Phys. Rev. Lett. **105**, 088304 (2010).
 [7] R. Dreyfus, J. Baudry, M. L. Roper, M. Fermigier, H. A. Stone, and J. Bibette, Nature (London) **437**, 862 (2005).
 [8] P. Tierno, R. Golestanian, I. Pagonabarraga, and F. F. Sagues, J. Phys. Chem. B **112**, 16525 (2008).
 [9] I. S. Aranson and L. S. Tsimring, Rev. Mod. Phys. **78**, 641 (2006).
 [10] S. Ramaswamy, Annu. Rev. Condens. Matter Phys. **1**, 323 (2010).
 [11] B. Kaehr and J. B. Shear, Lab Chip **9**, 2632 (2009).
 [12] G. Volpe, I. Buttinoni, D. Vogt, H. J. Kümmerer, and C. Bechinger, Soft Matter **7**, 8810 (2011).
 [13] D. L. Englert, M. D. Manson, and A. Jayaraman, Nature Protocols **5**, 864 (2010).
 [14] G. Mino, T. E. Mallouk, T. Darnige, M. Hoyos, J. Dauchet, J. Dunstan, R. Soto, Y. Wang, A. Rousselet, and E. Clement, Phys. Rev. Lett. **106**, 048102 (2011).
 [15] S. E. Hulme, W. R. DiLuzio, S. S. Shevkoplyas, L. Turner, M. Mayer, H. C. Berg, and G. M. Whitesides, Lab Chip **8**, 1888 (2008).
 [16] S. R. McCandlish, A. Baskaran, and M. F. Hagan, Soft Matter **8**, 2527 (2012).
 [17] M. B. Wan, C. J. Olson Reichhardt, Z. Nussinov, and C. Reichhardt, Phys. Rev. Lett. **101**, 018102 (2008).
 [18] R. DiLeonardo, L. Angelani, D. DellArciprete, G. Ruocco, V. Iebba, S. Schippa, M. P. Conte, F. Mecarini, F. D. Angelis, and E. D. Fabrizio, Proc. Natl. Acad. Sci. U.S.A. **107**, 9541 (2010).
 [19] A. Sokolov, M. M. Apodaca, B. A. Grzyboski, and I. S. Aranson, Proc. Natl. Acad. Sci. U.S.A. **107**, 969 (2010).
 [20] L. Angelani, R. DiLeonardo, and G. Ruocco, Phys. Rev. Lett. **102**, 048104 (2009).
 [21] H. H. Wensink and H. Löwen, Phys. Rev. E **78**, 031409 (2008).
 [22] M. M. Tirado, J. G. de la Torre, and C. L. Martinez, J. Chem. Phys. **81**, 2047 (1984).
 [23] J. Tailleur and M. E. Cates, Phys. Rev. Lett. **100**, 218103 (2008).

[24] K. Drescher, J. Dunkel, L. H. Cisneros, S. Ganguly, and R. E. Goldstein, Proc. Natl. Acad. Sci. U.S.A. **108**, 10940 (2011).

[25] V. Narayan, S. Ramaswamy, and N. Menon, Science **317**, 105 (2007).

[26] L. H. Cisneros, R. Cortez, C. Dombrowski, R. E. Goldstein, and J. O. Kessler, Exp. Fluids **43**, 737 (2007).

[27] D. Volfson, A. Kudrolli, and L. S. Tsimring, Phys. Rev. E **70**, 051312 (2004).

[28] E. Gauger and H. Stark, Phys. Rev. E **74**, 021907 (2006).

[29] I. O. Götze and G. Gompper, Phys. Rev. E **82**, 041921 (2010).

[30] J. K. G. Dhont, *An Introduction to the Dynamics of Colloids* (Elsevier, Amsterdam, 1996).